TSINGHUA SCIENCE AND TECHNOLOGY
ISSN 1007-0214 14/16 pp619–629
DOI: 10.26599/TST.2021.9010023
Volume 27, Number 3, June 2022

Visual Information Based Social Force Model for Crowd Evacuation

Wenhan Wu, Maoyin Chen, Jinghai Li, Binglu Liu, Xiaolu Wang, and Xiaoping Zheng*

Abstract: With the increase in large-scale incidents in real life, crowd evacuation plays a pivotal role in ensuring the safety of human crowds during emergency situations. The behavior patterns of crowds are well rendered by existing crowd dynamics models. However, most related studies ignore the information perception of pedestrians. To overcome this issue, we develop a visual information based social force model to simulate the interpretable evacuation process from the perspective of visual perception. Numerical experiments indicate that the evacuation efficiency and decision-making ability promote rapidly within a small range with the increase in unbalanced prior knowledge. The propagation of acceleration behavior caused by emergencies is asymmetric due to the anisotropy of visual information. Therefore, this model effectively characterizes the effect of visual information on crowd evacuation and provides new insights into the information perception of individuals in complex scenarios.

Key words: crowd evacuation; visual information; social force model; decision-making

1 Introduction

In light of the increasing size and frequency of mass events in public places[1], ignoring the existence of crowd safety is becoming extremely difficult[2, 3]. Effective crowd management[4] and evacuation schemes[5] are essential to reduce casualties and property loss during accidents[6]. For the purpose of revealing the underlying mechanism[7] of crowd motion in real life, many models[8] of pedestrian behavior have been proposed. As one of the most well-known crowd dynamics models, the social force model (SFM)[9, 10] is based on Newtonian mechanics, successfully accounting for a number of self-organization phenomena[11, 12] found in empirical observations. However, the information interaction of pedestrians, which can be regarded as valid prior knowledge[13], is not fully utilized in SFM. In addition, little is known about the quantification of the impact of information perception.

Existing studies recognize the significant role of information perception, especially for visual information[14, 15], in understanding crowd evacuation[16]. Visual information-driven models are established on the basis of psychological or physiological theories. Lemasson et al.[17] proposed a simplified retinal model to characterize the influence of neighbors based on neurobiological research results of information perception. Moreover, other crowd motion models, such as the lattice hydrodynamic model considering the visual field effect[18], the perceived cost potential field cellular automata model[19], and the heuristics-based SFM[20, 21], have been developed to incorporate the impact of visual information. Nevertheless, most of these models involve the influence of several factors, such as the view field and blind angle, and lack the systematic analysis for the impact of visual information on individual behaviors in evacuation scenarios.

With the increase in quantitative data describing social interactions, recent studies have provided important guidance on visual information-driven models.

• Wenhan Wu, Maoyin Chen, Jinghai Li, Binglu Liu, Xiaolu Wang, and Xiaoping Zheng are with the Department of Automation, Tsinghua University, Beijing 100084, China. E-mail: wwh19@mails.tsinghua.edu.cn; mychen@mail.tsinghua.edu.cn; ljhai725@163.com; liubl17@mails.tsinghua.edu.cn; wangxlu@mail.tsinghua.edu.cn; asean@mail.tsinghua.edu.cn.

* To whom correspondence should be addressed.
Manuscript received: 2021-01-05; revised: 2021-03-01; accepted: 2021-03-15

Rosenthal et al.[22] calculated the view fields of individuals and constructed a visual interaction network by investigating the behavioral changes in golden shiners. Collignon et al.[23] illustrated the stochastic vision based model inspired by zebrafish collective behavior in heterogeneous environments. Lin et al.[24] established the visually guided obstacle flight model inspired by bird eyes. Although the above visual information-driven models are adopted to explore simple behavior patterns[25, 26] in ideal environments, whether they are appropriate for explicating the latent laws of crowd evacuation remains unsettled.

This paper proposes a visual information based SFM (VISFM) to surmount the weakness of existing models on information perception. The visual perception mechanisms are effectively integrated into this model, which is developed as a framework to simulate intelligent behavior patterns of pedestrians without additional assumptions. Numerical simulation experiments indicate that the VISFM is interpretable and can achieve the intelligent behavior of crowds in complex scenarios. The increase in unbalanced prior knowledge is beneficial for the enhancement of evacuation efficiency and decision-making ability. Moreover, the propagation of accelerated behavior is asymmetric due to the anisotropy of visual information.

The rest of this paper is organized as follows. In Section 2, the VISFM is proposed. Section 3 provides the corresponding numerical experiments and analyzes the effect of visual information on crowd evacuation. Finally, Section 4 describes the discussion and future research topics.

2 Method

2.1 Model expression

Considering the impact of visual information, the desired direction of pedestrians depends on their own decisions and the neighbor information in their visual fields. On the one hand, $es_i\ (t)$ is defined as the desired direction based on prior knowledge and scene information. On the other hand, $ev_i\ (t)$ denotes the desired direction based on neighbor information. Hence, the desired direction of pedestrian i is expressed by the following:

$$e_i^0\ (t) = \omega_e \cdot ev_i\ (t) + (1-\omega_e)\, es_i\ (t) \tag{1}$$

where ω_e represents the weighting coefficient presenting a tradeoff between the above two factors. When the pedestrian understands the escape path, ω_e is close to 0; otherwise, it is close to 1 when the pedestrian follows the behavior of neighbors. In our case, ω_e is obtained by sampling with the sigmoid function in accordance with its own decision confidence f_s and neighbor information confidence f_n, which is given as follows:

$$\omega_e = \frac{1}{1+\mathrm{e}^{-k_r r}} \tag{2}$$

where k_r indicates its slope, and r is a random variable following the uniform distribution $r \sim U\ (-10-f_s+f_n, 10-f_s+f_n)$.

We assume that $eso_i\ (t)$ and $esv_i\ (t)$ represent the correct escape direction corresponding to the fastest decline of the static ground field and the desired direction based on visual information, respectively. Thus, $es_i\ (t)$ corresponds to the correct escape direction $eso_i\ (t)$ when pedestrian i is familiar with the escape route information, whereas $es_i\ (t)$ refers to the desired direction $esv_i\ (t)$ judged by the visual information.

Additionally, $ev_i\ (t)$ is the desired direction based on neighbor information. In the retinal model, individuals select the average value of the occlusion boundary as the desired movement direction[27]. Inspired by this model, the visual occlusion curves are adopted to indicate the approximate direction of neighbor distribution. Suppose the visual occlusion curve $g\left(\theta_{ij}\right)$ is the number of neighbors observed from each angle. Individuals with heterogenous heights are blocked to varying degrees, resulting in different visual occlusion curves. Based on the visual occlusion curve, the average angle of neighbor distribution direction is calculated as follows:

$$\delta_i^{(t)} = \frac{1}{N_I}\sum_{j=1}^{N_I}\left[\theta_{ij}\cdot g\left(\theta_{ij}\right)\right] \tag{3}$$

where N_I is the number of neighbors in the view field.

From the above-mentioned analysis, the visual occlusion curve and the alignment effect in the crowd are comprehensively considered to form the desired direction $ev_i\ (t)$ based on the neighbor information:

$$ev_i(t) = \omega_n e_i^{\delta}(t) + (1-\omega_n)\cdot\left\langle e_i^0\ (t-1)\right\rangle \tag{4}$$

where $e_i^{\delta}(t) = [\cos(\delta_i^{(t)}), \sin(\delta_i^{(t)})]$ is the direction vector of $\delta_i^{(t)}$, $\left\langle e_i^0\ (t-1)\right\rangle$ denotes the average direction of neighbors in the previous step, and ω_n is regarded as a weighting factor, with a general approximation of $\omega_n = 0.5$.

Given that the capability to avoid obstacles of visual information, visual heuristic rules[21] are used to modify the escape expectation, and the desired direction and desired speed are obtained by minimizing the collision

loss function:

$$d(\alpha) = d_{\max}^2 + f(\alpha)^2 - 2d_{\max} f(\alpha) \cos\left(\alpha_i^0(t) - \alpha\right) \tag{5}$$

where α_i^0 is the angle corresponding to the desired direction $e_i^0(t)$, and the potential collision distance $f(\alpha)$ of angle α is given by the following:

$$f(\alpha) = \min\left\{f_j(\alpha), f_b(\alpha)\right\} \tag{6}$$

where $f_j(\alpha)$ is the distance to collide with pedestrian j, and $f_b(\alpha)$ is the distance to collide with obstacles or walls. If no collision appears, the collision distance is the view field distance $d_{\max}$.

Thereby, the optimal escape direction $e_i^v(t)$, corresponding to the optimal escape angle $\hat{\alpha}_i$, is deduced by minimizing the collision loss function. Meanwhile, the optimal escape speed $v_i^v(t)$ is given as follows:

$$v_i^v(t) = \min\left\{v_i^0(t), \frac{d_h}{\tau}\right\} \tag{7}$$

where $v_i^0(t)$ is the escape desired speed, d_h represents the distance between pedestrian i and the nearest obstacle, and τ is related to a certain relaxation time.

In view of the aforementioned derivation and discussion, we develop a VISFM incorporating the impact of visual information. The combined effect of forces leads to dynamic changes in the pedestrian acceleration, which is expressed by the nonlinear coupled Langevin equations of motion:

$$m_i \frac{\mathrm{d}v_i(t)}{\mathrm{d}t} = f_{iv} + \sum_{j(\neq i)} f_{ij} + \sum_{w} f_{ib} \tag{8}$$

where f_{iv}, f_{ij}, and f_{ib} represent a self-driven force based on the visual information, a force due to an agent-to-agent interaction, and the interaction force between the pedestrian and obstacles, respectively.

Herein, the self-driven force based on visual information is written in the following form:

$$f_{iv} = m_i \frac{v_i^v(t)\, e_i^v(t) - v_i(t)}{\tau} \tag{9}$$

where m_i is the mass of pedestrian i, $v_i^v(t)$ and $e_i^v(t)$ represent the optimal escape speed and direction by minimizing the collision loss function, respectively.

The interaction force f_{ij} between pedestrians i and j is referred to SFM and expressed as follows:

$$f_{ij} = kg\left(r_{ij} - d_{ij}\right) n_{ij} + \kappa g\left(r_{ij} - d_{ij}\right) \Delta v_{ji}^t t_{ij} \tag{10}$$

where $kg\left(r_{ij} - d_{ij}\right) n_{ij}$ and $\kappa g\left(r_{ij} - d_{ij}\right) \Delta v_{ji}^t t_{ij}$ correspond to the body force and sliding friction force from pedestrians i to j, respectively. Here, r_{ij} and d_{ij} refer to the radius sum and the distance between the centroids of pedestrian i and j, respectively, and $g(x)$ is zero if the two pedestrians do not touch each other; otherwise, it equals to x. For the body force, k denotes the body elasticity coefficient and n_{ij} is the normalized vector pointing from pedestrians j to i. For the sliding friction force, κ is the sliding friction coefficient and t_{ij} represents the tangential direction.

The physical force f_{ib} of surrounding obstacles or walls on pedestrians is similar to the expression of f_{ij}:

$$f_{ib} = kg\left(r_i - d_{ib}\right) n_{ib} - \kappa g\left(r_i - d_{ib}\right)\left(v_i \cdot t_{ib}\right) t_{ib} \tag{11}$$

where $kg\left(r_i - d_{ib}\right) n_{ib}$ and $\kappa g\left(r_i - d_{ib}\right)\left(v_i \cdot t_{ib}\right) t_{ib}$ represent the body force and sliding friction force from pedestrian i to obstacles or walls, respectively. Here, d_{ib} and n_{ib} represent the distance and normalized vector perpendicular from pedestrian i to obstacles or walls, and t_{ib} is the tangential direction.

2.2 Dynamic update of parameters

In the previous section, the detailed expression of VISFM is developed. Here, we introduce the dynamic update of parameters in this model. The psychological states of pedestrians are affected by visual information perception, which may lead to changes in certain parameters.

On the one hand, pedestrians promote their desired speed to escape as the urgency increases from empirical observations. Figure 1 shows the division of hazardous areas based on this phenomenon. In the first-level dangerous area, pedestrian i immediately moves away from the danger source by increasing the desired speed by $k_{d_1} v_i^0(t)$. The second-level dangerous area is a visible area of the danger source, where pedestrian i increases the desired speed by $k_{d_2} v_i^0(t)$ and maintains it to escape, and the desired direction is the original

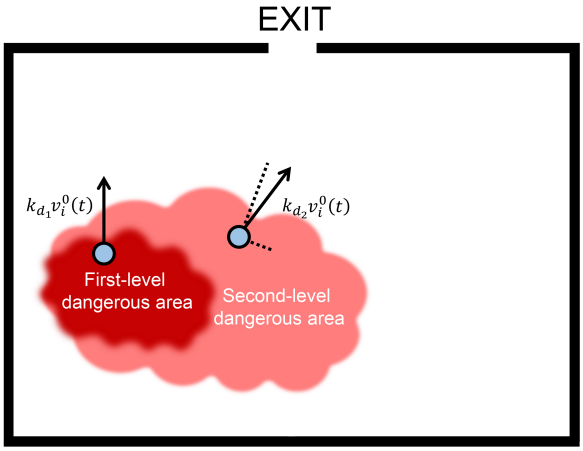

Fig. 1 Division of hazardous areas—the darker color refers to the first-level dangerous area, whereas, the lighter color corresponds to the second-level dangerous area.

desired direction deviates from the danger source. Note that $k_{d_1} > k_{d_2} > 1$ in this case.

On the other hand, the weighting coefficient ω_e, the trust level of self-decision f_s, and neighbor information f_n are also updated reasonably based on the psychological states of pedestrians. The trust level of self-decision f_s is affected by prior knowledge and scene information, such as evacuation signs and terrain information. If the pedestrian has prior knowledge ($sd_i = 1$), then f_s is extremely high, and $\omega_e \to 0$; otherwise, the prior knowledge is ignored ($sd_i = 0$), and f_s and ω_e are determined by the scene information in Fig. 2.

In addition, the trust level of neighbor information f_n is affected by the characteristics of neighbor distribution, including the number and direction of neighbors, which is given by the following:

$$f_n = \begin{cases} 6, & N > 1 \text{ and } \left|\sum e_j \Big/ N\right| \geqslant 0.7; \\ 3, & N = 1 \text{ or } \left|\sum e_j \Big/ N\right| < 0.7; \\ 0, & N < 1 \end{cases} \tag{12}$$

where N denotes the number of total pedestrians, and $\sum e_j$ corresponds to the sum of direction angles of neighbors.

For simplicity, the detailed simulation steps and parameters update of VISFM are summarized in the following procedure:

Step 1: Initialize parameters based on the pedestrians distributed in the scene.

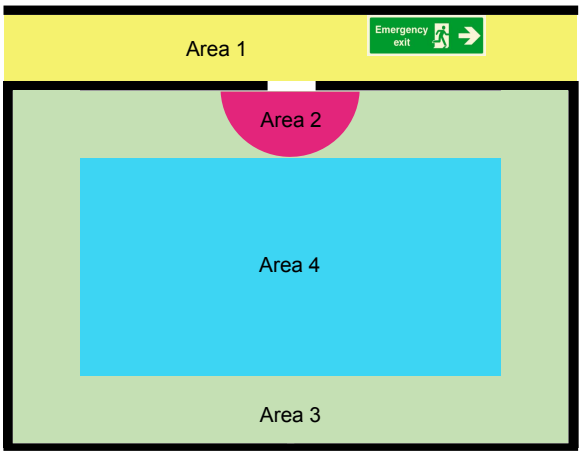

Fig. 2 Schematic of the weighting coefficient ω_e and the trust level of self-decision f_s affected by the scene information. In area 1, $f_s = 6$ when the evacuation sign can be observed. In area 2, $\omega_e = 0$ if an evacuation sign exists in the local exit; otherwise, $f_s = 6$. In area 3, $f_s = 3$ when the pedestrian can discover the wall or a corner. In area 4, $f_s = 0$ for the open area.

Step 2: Check remaining pedestrians. If all pedestrians left the scene, go to Step 7.

Step 3: Express multidimensional features of visual information.

Step 4: Dynamic update parameters v_i^0, ω_e, f_s, and f_n.

Step 5: Calculate self-driven force based on visual information.

Step 6: Update the positions of pedestrians with the VISFM and then go to Step 2.

Step 7: Finish the simulation.

For the above-mentioned parameters, we mainly consider the influence of visual information on the mentality involving the cognition of scene information, such as local exits, escape signs, and neighbor features. For the position of pedestrians, through the obstacle avoidance behavior generated by visual information, the escape expectation is obtained from prior knowledge, scene information, and neighbor information. Then, the positions of pedestrians are updated by our model.

3 Results and Discussion

3.1 Effect of visual perception on crowd evacuation

In this section, we simulate crowd evacuation in the subway station scene (90 m length and 22.5 m width). Figure 3a depicts the detailed map of the subway station scene, and the corresponding static ground field is shown in Fig. 3b, where the correct escape direction is always the fastest direction decreasing along the navigation ground field. Based on empirical data, the ordinary pedestrian in our model is regarded as a circular particle

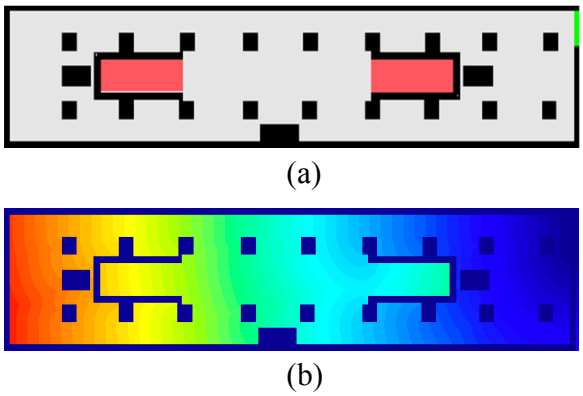

Fig. 3 2D floor plan of a subway station scene (90 m length and 22.5 m width). (a) Detailed map of the subway station scene. Red and green areas correspond to the entry and exit, respectively. (b) Static ground field of the subway station scene. The blue and red areas indicate the areas closer to and farther from the exit, respectively.

with radius $r \in [0.25\,\text{m}, 0.35\,\text{m}]$, mass $m = 80\,\text{kg}$, initial desired speed $v_i^0 = 0.8\,\text{m}\cdot\text{s}^{-1}$, and relaxation time $\tau = 0.5$ s. Additionally, the time step $\Delta t = 0.04$ s and scene visibility $d_{\max} = 5$ m are selected, and the height of the crowd is uniformly distributed in the interval $[1.4\,\text{m}, 2\,\text{m}]$.

Figure 4 shows the comparison of the evacuation processes simulated by SFM and VISFM in the subway station scene. The temporal evolution curves of the number of exited pedestrians in Fig. 4a reveal that the evacuation efficiencies simulated by both models are nearly consistent. Thus, our model effectively simulates the pedestrian evacuation process. From the spatial dimension, however, evident differences exist in the spatial distribution of crowd performed by SFM and VISFM. Figure 4b illustrates snapshots of crowd evacuation simulated by SFM and VISFM at $t = 53$ s. The crowd simulated by SFM is arranged in a relatively neat queue, whereas the distribution of crowd simulated by VISFM is more decentralized, which is more consistent with empirical observations.

Although the evacuation efficiencies simulated by SFM and VISFM are similar, VISFM performs looser crowd distribution and higher space utilization in terms of spatial dimension. This indicates that pedestrians adjust their movement directions based on visual information, which is more interpretable and can achieve the intelligent behavior of crowds in complex scenarios.

3.2 Analysis of crowd evacuation with unbalanced prior knowledge

The same as the experimental scene in the previous section, we explore the effect of unbalanced prior knowledge on crowd evacuation. For pedestrians who possess prior knowledge about the evacuation path, $sd_i = 1$; otherwise, other pedestrians in the crowd are given $sd_i = 0$. To characterize the unbalanced degree of prior knowledge, we express the proportion of pedestrians who have prior knowledge using the following:

$$p_{PK} = \frac{1}{N}\sum_{i=0}^{N} sd_i \tag{13}$$

In the following simulations, we analyze the impact of unbalanced prior knowledge on evacuation efficiency and decision-making ability.

Figure 5 illustrates the influence of unbalanced prior knowledge on evacuation efficiency. As shown in Fig. 5a, the slopes of multiple curves are distinct when p_{PK} varies from 0.0 to 1.0. Notably, the increased proportion of pedestrians who have prior knowledge greatly promotes evacuation efficiency. Figure 5b intuitively illustrates the effect of unbalanced prior knowledge by conducting 100 trials to avoid accidental results. With the increase in the proportion p_{PK}, the number of exited pedestrians within 120 s increases, causing the average evacuation time to decrease significantly. The evacuation efficiency increases at a fast rate when $p_{PK} \leqslant 0.3$ (gray area) but at a slow rate when $p_{PK} > 0.3$. The findings preliminarily demonstrate that when p_{PK} is higher than 0.3, although others are unfamiliar with the evacuation path, the majority of them successfully escape by obtaining the navigation information of their neighbors through visual perception.

To evaluate the impact of unbalanced prior knowledge on the decision-making ability, we define the ratio of average effective time η_E, the average escape direction declination angle θ_d, and the proportion of

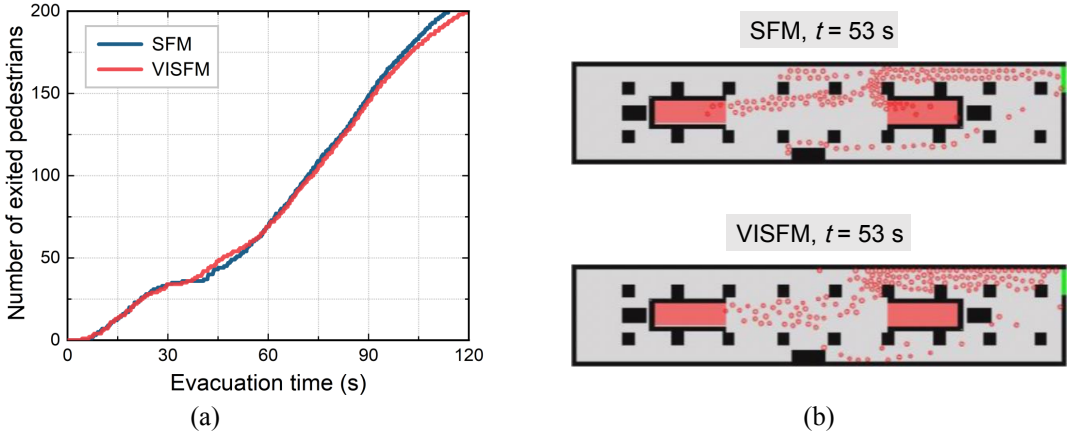

Fig. 4 Comparison of evacuation processes simulated by SFM and VISFM in the subway station scene. (a) The number of exited pedestrians, as shown by the temporal evolution curves of SFM and VISFM during the evacuation process. (b) Snapshots of crowd evacuation simulated by SFM and VISFM at $t = 53$ s.

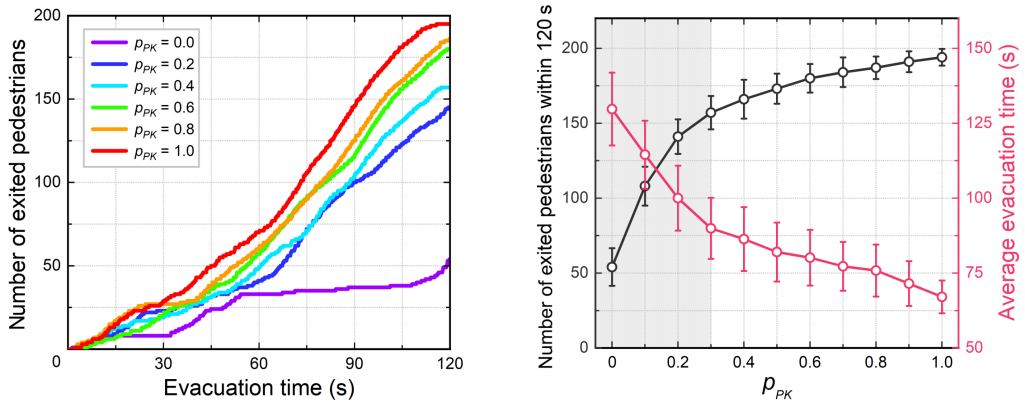

(a) (b)

Fig. 5 Influence of unbalanced prior knowledge on the evacuation efficiency. (a) The number of exited pedestrians shows as a function of the evacuation time; different colors correspond to various proportions of the pedestrians who have prior knowledge. (b) Evacuation efficiency curves of varying unbalanced prior knowledge. The black and red curves represent the number of exited pedestrians within 120 s and average evacuation time, respectively. The shape points and error bars denote the mean and standard deviation based on 100 trials.

steps followed by neighbors $c_{\omega e}$ (Appendix A). As the prior knowledge proportion p_{PK} increases (Fig. 6), the ratio of average effective time η_E improves, whereas the average escape direction declination angle θ_d and the proportion of steps followed by neighbors $c_{\omega e}$ decrease, indicating that pedestrians familiar with the evacuation path prefer to escape relying on their own decisions. Hence, the increased proportion of pedestrians who possess prior information promotes the crowd's decision-making ability due to the sharing of navigation information.

Figure 7 shows the influence of unbalanced prior knowledge on the decision-making ability under different numbers of pedestrians. In Figs. 7a and 7c, the ratio of average effective time η_E and the proportion of steps followed by neighbors $c_{\omega e}$ increase as the number of pedestrians increases owing to the large probabilities of pedestrians acquiring visual information, which leads

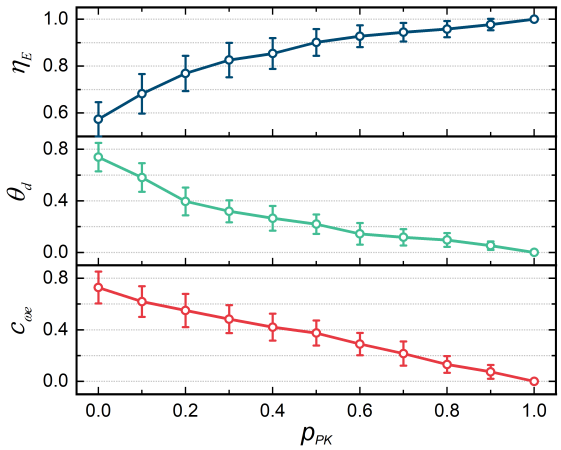

Fig. 6 Influence of unbalanced prior knowledge on the decision-making ability. The evaluation indicators η_E, θ_d, and $c_{\omega e}$ show as a function of the prior knowledge proportion p_{PK}. The shape points and error bars denote the mean and standard deviation based on 100 trials.

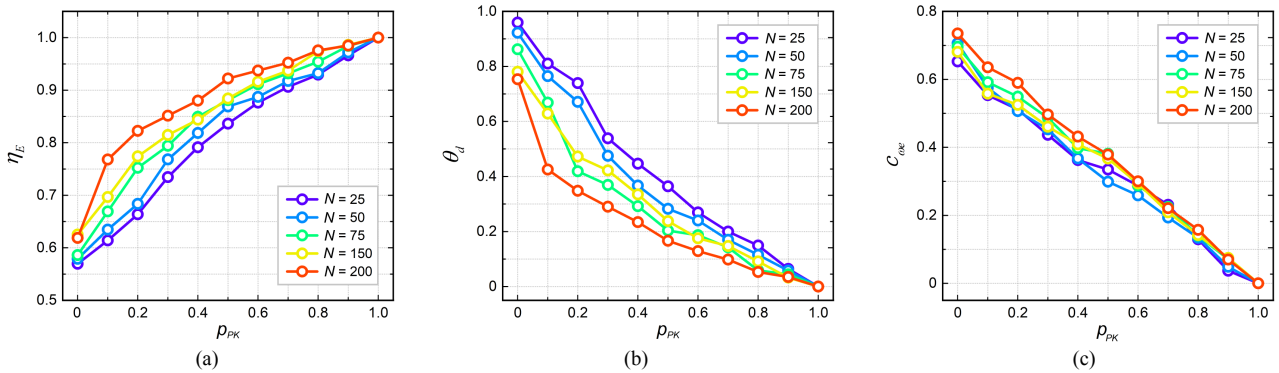

(a) (b) (c)

Fig. 7 Influence of unbalanced prior knowledge on decision-making ability under different numbers of pedestrians. (a) Ratio of average effective time η_E. (b) Average escape direction declination angle θ_d. (c) Proportion of steps followed by neighbors $c_{\omega e}$. The shape points denote the mean based on 100 trials.

to the effective propagation of navigation information. In addition, a high crowd density corresponds to a small average escape direction declination angle θ_d (Fig. 7b). This result reveals that increasing the number of pedestrians is beneficial for the decision-making ability of pedestrians.

3.3 Asymmetric propagation of accelerated behavior

Our model describes that pedestrian state parameters are affected by visual information, which can be utilized to simulate and analyze the propagation of accelerated behavior in the crowd caused by emergencies. Given that a pedestrian may follow neighbors when he observes crowd acceleration, a visual interaction network[22] is constructed to describe the propagation of accelerated behavior among individuals (Appendix B).

Figure 8 shows the process of acceleration behavioral contagion in the unidirectional flow scene (80 m length and 10 m width). On the one hand, when the danger source appears behind the crowd in Fig. 8a, individuals behind the crowd perform remarkably accelerated behavior at the initial time ($t = 3.56$ s). The propagation process is interrupted until several accelerated individuals surpass other individuals from the side ($t = 14.08$ s and $t = 16.28$ s), which leads to the spread of the accelerated behavior to the entire group in a short time ($t = 17.20$ s). On the other hand, when the danger source is in front of the crowd, pedestrians easily discover the danger source by visual perception ($t = 1.12$ s and $t = 1.24$ s). Thereby, the accelerated behavior quickly spreads from individuals closer to the danger source in the entire group ($t = 2.32$ s and $t = 3.28$ s), shown in Fig. 8b.

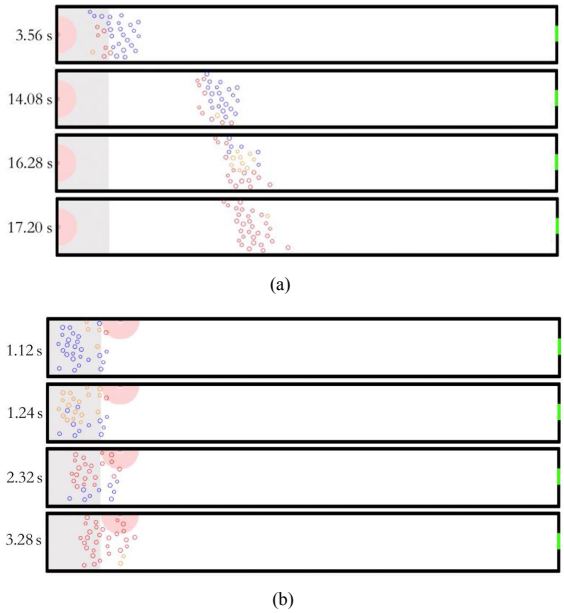

Fig. 8 Process of acceleration behavioral contagion in the unidirectional flow scene (80 m length and 10 m width). (a) Danger source appearing behind the crowd. (b) Danger source on the front side of the crowd. The blue, orange, and red circles represent the normal, critical accelerated, and accelerated individuals, respectively.

To quantitatively explore the influence of the location of the danger source on the accelerated behavior, we set up four different danger source areas in the unidirectional flow scene. Figure 9 depicts the danger source behind the crowd, on the side of the crowd, on the front side of the crowd, and in front of the crowd, where red areas correspond to the different locations of the danger source. The crowd is randomly distributed on the left side of the unidirectional flow scene (gray area), escaping toward the exit on the right side (green strip area).

Figure 10 illustrates the accelerated behavior of pedestrians under the four different situations. When the number of pedestrians is fixed as $N = 30$ (Figs. 10a–10d), the propagation speed of the accelerated behavior gradually increases as the danger source moves forward. A similar phenomenon is observed in Figs. 10e–10h where the number is increased by $N = 50$, indicating the propagation of accelerated behavioral is asymmetric due to the anisotropy of visual information. Moreover, with the increase in crowd density, the propagation speed of the accelerated behavior slows down if the danger source is behind the crowd, but it enhances when the danger source is on the side of the crowd. This condition is observed because the increase in the crowd density

Fig. 9 Location of danger source in the unidirectional flow scene. (a) Danger source behind the crowd. (b) Danger source on the side of the crowd. (c) Danger source on the front side of the crowd. (d) Danger source in front of the crowd.

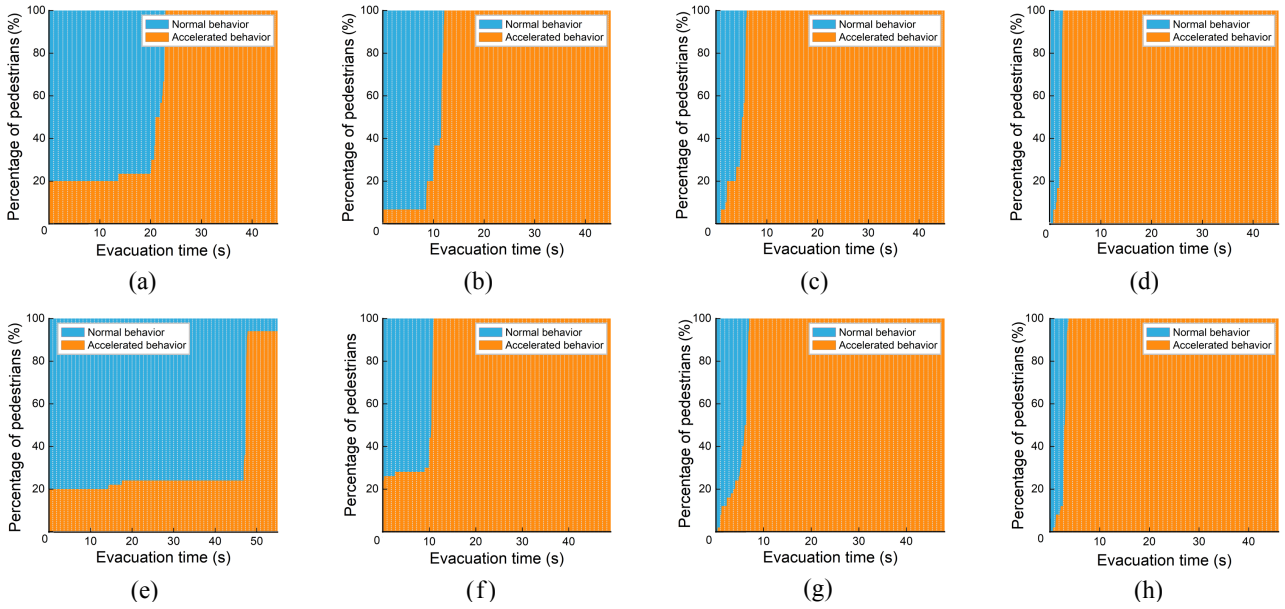

Fig. 10 Influence of the location of danger source on the accelerated behavior. (a)–(d) Evacuation process of 30 pedestrians for the danger source behind the crowd (a), on the side of the crowd (b), on the front side of the crowd (c), and in front of the crowd (d). (e)–(h) Evacuation process of 50 pedestrians for the danger source behind the crowd (e), on the side of the crowd (f), on the front side of the crowd (g), and in front of the crowd (h).

may hinder the surpassing of pedestrians in the rear and reduce the propagation speed of information to the front. However, the propagation speed from the side to other directions will be promoted.

4 Conclusion

In this paper, we use multidimensional visual information to construct a VISFM innovatively. By conducting numerical experiments in different interaction scenarios, several prime and interesting conclusions are summarized as follows:

(1) Compared with SFM, our model is more interpretable and realistic for simulating crowd evacuation processes in complex scenarios.

(2) The VISFM effectively characterizes the spontaneous evacuation process with unbalanced prior knowledge, demonstrating that evacuation efficiency and decision-making ability are promoted as the proportion of pedestrians with prior knowledge increases.

(3) The propagation of accelerated behavior is asymmetric due to the anisotropy of visual information, and crowd density has a certain effect on the propagation process.

Although VISFM involves the visual information perception of pedestrians, certain limitations still exist in this model. How to enhance the generality and accuracy of VISFM deserves in-depth consideration. Future research should pay attention to the following points: First, heterogeneous prior knowledge can be designed to explore the impact of different personnel structures on the evacuation process. Second, our model may be applied in complex scenarios to analyze the influence of the crowd distribution[28], distribution of obstacles[29], etc. In addition, visual interaction networks will be used to describe other state changes or behavioral propagation recognized by visual perception. Therefore, we expect that this model can stimulate the generation of more effective evacuation models, which will provide new insights into the field of crowd dynamics.

Appendix

A Evaluation indicators

Several evaluation indicators are defined to quantitatively analyze the effect of unbalanced prior knowledge on the decision-making ability.

First, the step is considered to be effective when the deviation angle between the actual and correct escape directions is limited to 20°. The average effective time t_E corresponds to the mean effective step time of all pedestrians and is calculated as follows:

$$t_E = \frac{1}{N}\sum_{i=1}^{N}\sum_{s=1}^{S_i} I\left(\arccos\left(\frac{e_i^s \cdot ec_i^s}{\left|e_i^s\right| \cdot \left|ec_i^s\right|}\right) < \frac{\pi}{9}\right) \cdot \Delta t \tag{A1}$$

where $I(\cdot)$ denotes the indicator function, S_i holds the total steps of pedestrian i, Δt denotes the time step, e_i^s is the escape direction in step s, and ec_i^s corresponds to the correct escape direction. Assuming that t_T is the average time, the ratio of average effective time is calculated by the following:

$$\eta_E = \frac{t_E}{t_T} \tag{A2}$$

Then, the deflection angle of escape direction is computed as the average value of the deflection angle between the correct and actual escape directions, which indicates the decision-making ability. The average escape direction declination angle is given by the following:

$$\theta_d = \frac{1}{N}\sum_{i=1}^{N}\frac{1}{S_i}\sum_{s=1}^{S_i}\arccos\left(\frac{e_i^s \cdot ec_i^s}{\left|e_i^s\right| \cdot \left|ec_i^s\right|}\right) \tag{A3}$$

Finally, the weighting coefficient is used to balance the information of self, neighbors, and scenes. The proportion of steps followed by neighbors $c_{\omega e}$ is defined below to express this subsequent effect:

$$c_{\omega e} = \frac{1}{N}\sum_{i=1}^{N}\frac{1}{S_i}\sum_{s=1}^{S_i} I\left(\omega_e^s > 0.5\right) \tag{A4}$$

Herein, if pedestrians prefer to follow neighbors to escape in step s, then $\omega_e^s > 0.5$; otherwise, $\omega_e^s \leqslant 0.5$.

B Visual interaction network

According to the ranking based on the distance and angle of neighbors to pedestrian i, the response probability $p_{i,j}$ from pedestrians i to j is given by the following:

$$p_{i,j} = \frac{1}{1 + \mathrm{e}^{-\beta_1 - \beta_2 LMD - \beta_3 AR}} \tag{A5}$$

where β_1, β_2, and β_3 are constants, LMD is the logarithm of the distance between pedestrians i and j, AR is the angle ranking of pedestrian j in the view field of pedestrian i. In the case of the response probability, the propagation model of the visual interaction network is expressed by the following:

$$D_i^{(t)} = \begin{cases} 1, & \sum_{j=1}^{N}\gamma_{i,j} > \phi_i; \\ 0, & \sum_{j=1}^{N}\gamma_{i,j} \leqslant \phi_i \end{cases} \tag{A6}$$

where $D_i^{(t)} = 1$ denotes the accelerated state; otherwise, $D_i^{(t)} = 0$ represents the normal state. The selection function of response probability $\gamma_{i,j}$ is given by the following:

$$\gamma_{i,j} = I(p_{i,j} D_j^{(t-1)} > u_{i,j}) \tag{A7}$$

where $D_j^{(t-1)}$ is the state of neighbor j at time $t-1$. The parameters $u_{i,j}$ and ϕ_i are determined by the propagation model, which has three forms, namely, random propagation, numerical propagation, and fractional propagation.

In the random propagation model, $\phi_i = 1$. A neighbor of pedestrian i is randomly selected as the responding neighbor, and $u_{i,j} \in [0, 1]$ is defined as a random number. For the remaining neighbors, $u_{i,j} = 1$. The pedestrian i randomly selects a neighbor as a response behavior.

In the numerical propagation model, $\phi_i = n_c$ where n_c is a fixed numerical threshold. For all unblocked neighbors in the view field of pedestrian i, $u_{i,j} \in [0, 1]$ is a random number; for other neighbors, $u_{i,j} = 1$. The pedestrian i responds to the behavior state only when the number of responding neighbors exceeds the fixed threshold n_c.

In the fractional propagation model, $\phi_i = k_c M_i$ where k_c is the fixed fractional threshold, and M_i is the number of neighbors. For all unblocked neighbors in the view field of pedestrian i, $u_{i,j} \in [0, 1]$ is a random number; for other neighbors, $u_{i,j} = 1$. The pedestrian i responds to the behavior state only when the number of responding neighbors exceeds the fixed fractional threshold k_c.

Acknowledgment

This work was supported by the National Key Research and Development Program of China (No. 2020YFF0304900) and the National Major Scientific Research Instrument Development Project of China (No. 61927804).

References

[1] Q. S. Zhang, G. M. Zhao, and J. L. Liu, Performance-based design for large crowd venue control using a multi-agent model, *Tsinghua Science and Technology*, vol. 14, no. 3, pp. 352–359, 2009.

[2] A. Bottinelli, D. T. J. Sumpter, and J. L. Silverberg, Emergent structural mechanisms for high-density collective motion inspired by human crowds, *Phys. Rev. Lett.*, vol. 117, no. 22, p. 228301, 2016.

[3] J. L. Silverberg, M. Bierbaum, J. P. Sethna, and I. Cohen, Collective motion of humans in mosh and circle pits at heavy metal concerts, *Phys. Rev. Lett.*, vol. 110, no. 22, p. 228701, 2013.

[4] C. Martella, J. Li, C. Conrado, and A. Vermeeren, On current crowd management practices and the need for increased situation awareness, prediction, and intervention, *Safety Science*, vol. 91, pp. 381–393, 2017.

[5] M. N. A. Khalid and U. K. Yusof, Dynamic crowd evacuation approach for the emergency route planning problem: Application to case studies, *Safety Science*, vol. 102, pp. 263–274, 2018.

[6] F. Q. Tang and A. Z. Ren, Agent-based evacuation model incorporating fire scene and building geometry, *Tsinghua Science and Technology*, vol. 13, no. 5, pp. 708–714, 2008.

[7] H. J. Charlesworth and M. S. Turner, Intrinsically motivated

collective motion, *Proceedings of the National Academy of Sciences of the United States of America*, vol. 116, no. 31, pp. 15362–15367, 2019.
[8] X. P. Zheng, T. K. Zhong, and M. T. Liu, Modeling crowd evacuation of a building based on seven methodological approaches, *Building and Environment*, vol. 44, no. 3, pp. 437–445, 2009.
[9] D. Helbing and P. Molnár, Social force model for pedestrian dynamics, *Phys. Rev. E*, vol. 51, no. 5, pp. 4282–4286, 1995.
[10] D. Helbing, I. Farkas, and T. Vicsek, Simulating dynamical features of escape panic, *Nature*, vol. 407, no. 6803, pp. 487–490, 2000.
[11] L. Zhao, G. Yang, W. Wang, Y. Chen, J. P. Huang, H. Ohashi, and H. E. Stanley, Herd behavior in a complex adaptive system, *Proceedings of the National Academy of Sciences of the United States of America*, vol. 108, no. 37, pp. 15058–15063, 2011.
[12] W. J. Yu and A. Johansson, Modeling crowd turbulence by many-particle simulations, *Phys. Rev. E*, vol. 76, no. 4 Pt 2, p. 046105, 2007.
[13] M. Spering and H. M. Chow, Rapid assessment of natural visual motion integration across primate species, *Proceedings of the National Academy of Sciences of the United States of America*, vol. 115, no. 44, pp. 11112–11114, 2018.
[14] L. Y. Deng, M. Yang, Z. D. Liang, Y. S. He, and C. X. Wang, Fusing geometrical and visual information via superpoints for the semantic segmentation of 3D road scenes, *Tsinghua Science and Technology*, vol. 25, no. 4, pp. 498–507, 2020.
[15] J. J. Lin, L. Y. Liang, X. Han, C. Yang, X. G. Chen, and X. R. Gao, Cross-target transfer algorithm based on the volterra model of SSVEP-BCI, *Tsinghua Science and Technology*, vol. 26, no. 4, pp. 505–522, 2021.
[16] R. Bastien and P. Romanczuk, A model of collective behavior based purely on vision, *Science Advances*, vol. 6, no. 6, p. eaay0792, 2020.
[17] B. H. Lemasson, J. J. Anderson, and R. A. Goodwin, Collective motion in animal groups from a neurobiological perspective: The adaptive benefits of dynamic sensory loads and selective attention, *Journal of Theoretical Biology*, vol. 261, no. 4, pp. 501–510, 2009.
[18] H. Kuang, T. Chen, X. L. Li, and S. M. Lo, A new lattice hydrodynamic model for bidirectional pedestrian flow considering the visual field effect, *Nonlinear Dynamics*, vol. 78, no. 3, pp. 1709–1716, 2014.
[19] X. X. Jian, S. C. Wong, P. Zhang, K. Choi, H. Li, and X. N. Zhang, Perceived cost potential field cellular automata model with an aggregated force field for pedestrian dynamics, *Transportation Research Part C: Emerging Technologies*, vol. 42, pp. 200–210, 2014.
[20] M. Moussaïd, D. Helbing, S. Garnier, A. Johansson, M. Combe, and G. Theraulaz, Experimental study of the behavioural mechanisms underlying self-organization in human crowds, *Proceedings of the Royal Society B: Biological Sciences*, vol. 276, no. 1668, pp. 2755–2762, 2009.
[21] M. Moussaïd, D. Helbing, and G. Theraulaz, How simple rules determine pedestrian behavior and crowd disasters, *Proceedings of the National Academy of Sciences of the United States of America*, vol. 108, no. 17, pp. 6884–6888, 2011.
[22] S. B. Rosenthal, C. R. Twomey, A. T. Hartnett, H. S. Wu, and I. D. Couzin, Revealing the hidden networks of interaction in mobile animal groups allows prediction of complex behavioral contagion, *Proceedings of the National Academy of Sciences of the United States of America*, vol. 112, no. 15, pp. 4690–4695, 2015.
[23] B. Collignon, A. Séguret, and J. Halloy, A stochastic vision-based model inspired by zebrafish collective behaviour in heterogeneous environments, *Royal Society Open Science*, vol. 3, no. 1, p. 150473, 2016.
[24] H. T. Lin, I. G. Ros, and A. A. Biewener, Through the eyes of a bird: Modelling visually guided obstacle flight, *Journal of the Royal Society Interface*, vol. 11, no. 96, p. 20140239, 2013.
[25] A. Seyfried, B. Steffen, and T. Lippert, Basics of modelling the pedestrian flow, *Physica A: Statistical Mechanics and Its Applications*, vol. 368, no. 1, pp. 232–238, 2006.
[26] M. Moussaïd, N. Perozo, S. Garnier, D. Helbing, and G. Theraulaz, The walking behaviour of pedestrian social groups and its impact on crowd dynamics, *PLoS ONE*, vol. 5, no. 4, p. e10047, 2010.
[27] D. J. G. Pearce, A. M. Miller, G. Rowlands, and M. S. Turner, Role of projection in the control of bird flocks, *Proceedings of the National Academy of Sciences of the United States of America*, vol. 111, no. 29, pp. 10422–10426, 2014.
[28] B. W. Jin, J. H. Wang, Y. Wang, Y. M. Gu, and Z. R. Wang, Temporal and spatial distribution of pedestrians in subway evacuation under node failure by multi-hazards, *Safety Science*, vol. 127, p. 104695, 2020.
[29] N. Shiwakoti, X. M. Shi, and Z. R. Ye, A review on the performance of an obstacle near an exit on pedestrian crowd evacuation, *Safety Science*, vol. 113, pp. 54–67, 2019.

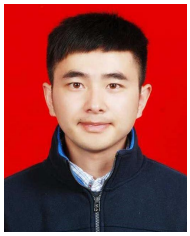

Jinghai Li received the BS degree in automation and the MS degree in control science and engineering from Tianjin University, Tianjin, China, in 2009 and 2016, respectively. He is currently pursuing the PhD degree in control science and engineering at Tsinghua University, Beijing, China. His current research interests include crowd dynamics, planning and control of robotic systems, and adaptive systems.

Wenhan Wu received the BS degree from Central South University, Changsha, China, in 2019. He is currently pursuing the PhD degree in control science and engineering at Tsinghua University, Beijing, China. His current research interests include crowd dynamics, collective behavior, emergency evacuation, and swarm intelligent robot.

Maoyin Chen received the BS degree in mathematics and the MS degree in control theory and control engineering from Qufu Normal University, Shandong, China, in 1997 and 2000, respectively, and the PhD degree in control theory and control engineering from Shanghai Jiao Tong University, Shanghai, China, in 2003. From 2003 to 2005, he was a postdoctoral researcher with the Department of Automation, Tsinghua University, Beijing, China. From 2006 to 2008, he visited Potsdam University, Potsdam, Germany, as an Alexander von Humboldt Research Fellow. Since October 2008, he has been an associate professor with the Department of Automation, Tsinghua University, Beijing, China. He has authored and coauthored over 100 peer-reviewed international journal papers. He has won the first prize in natural science (2011, ranked first) and the second prize (2019, ranked first) of CAA. His research interests include fault prognosis and complex systems.

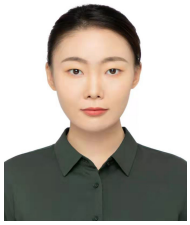

Binglu Liu received the BS and MS degrees in control science and engineering from Tsinghua University, Beijing, China, in 2017 and 2020, respectively. Her current research interests include crowd dynamics, emergency evacuation, and visual interactive network.

Xiaolu Wang received the PhD degree in control theory and control engineering from Beijing University of Chemical Technology in 2015. She is currently a research associate at the Department of Automation, Tsinghua University, Beijing, China. Her current research interests include crowd evacuation intervention mechanism, evacuation dynamics, and emergency management.

Xiaoping Zheng received the BS degree from Chengdu University of TCM, Chengdu, China, in 1995, and the PhD degree from Sichuan University, Chengdu, China, in 2003. From 2006 to 2013, he was a professor with the Institute of Safety Management, Beijing University of Chemical Technology, Beijing, China. He is currently a professor with the Department of Automation, Tsinghua University, Beijing, China. He was a 973 chief scientist in 2011 and recipient of the National Science Fund for Distinguished Young Scholars in 2012. His current research interests include large-scale crowd evacuation, evolutionary game theory, and terahertz technology.